DPP9 Overexpression in Clear Cell Renal Cell Carcinoma Causes Ferroptosis Suppression and Sorafenib Resistance Through the KEAP1–NRF2 Pathway

Kun Chang (changkungene@126.com)
Fudan University Shanghai Cancer Center
yingji Chen
Fudan University
Xuanzhi Zhang
Fudan University Shanghai Cancer Center
Wei Zhang
Shanghai Medical College, Fudan University
Bohan Zeng
Fudan University Shanghai Cancer Center
Bo Dai
Fujiang Xu
The Affiliated Hospital of Southwest Medical University https://orcid.org/0000-0002-7900-5319
Dingwei Ye
Fudan University Shanghai Cancer Center https://orcid.org/0000-0002-6761-5195
Chenji Wang
Fudan University https://orcid.org/0000-0002-5752-6439

Article

Keywords: oxidative stress, NRF2, KEAP1, ROS, ubiquitination

Posted Date: October 14th, 2022

DOI: https://doi.org/10.21203/rs.3.rs-2137070/v1

Abstract

The Kelch-like ECH-associated protein 1 (KEAP1)-nuclear factor erythroid 2-like 2 (NRF2) axis is the principal regulator of cellular responses against oxidative and electrophilic stressors. NRF2 hyperactivation, which is frequently observed in many types of cancers, promotes cancer initiation, progression, metastasis, and resistance to various therapies. Here, we determined that dipeptidyl peptidase 9 (DPP9) was markedly overexpressed at the mRNA and protein levels in clear cell renal cell carcinoma (ccRCC), and its overexpression was correlated with advanced tumour stage and poor prognosis in ccRCC patients. We searched for functional partners of DPP9 using protein affinity purification and determined that DPP9 interacts with KEAP1 via a conserved ESGE motif. The KEAP-NRF2 interaction was disrupted by DPP9, which competed with NRF2 for binding to KEAP1, independent of DPP9's enzymatic function. Overexpression of DPP9 stabilized the NRF2 protein, drove NRF2-dependent transcription, and reduced cellular relative oxygen species (ROS) levels. Moreover, DPP9 overexpression suppressed ferroptosis and caused resistance to sorafenib in ccRCC cells, which was largely dependent on the NRF2 transcriptional target-SLC7A11. Collectively, our findings indicated that the pathological process associated with the accumulation of DPP9 results in hyperactivation of the NRF2 pathway, which contributes to tumorigenesis and intrinsic drug resistance in ccRCC.

1. Introduction

The cell redox balance is the equilibrium between the generation and detoxification of ROS. Cells have several antioxidant defence systems that maintain ROS levels, including the transcription factor nuclear factor erythroid 2-like 2 (NRF2, encoded by NFE2L1). NRF2 orchestrates an elaborate transcriptional program in response to environmental cues arising from oxidants and electrophilic agents, allowing for adaptation and survival under stress conditions[1]. Therefore, NRF2 is pivotal for cellular protection against endogenous and exogenous insults. Under unstressed conditions, the NRF2 protein is polyubiquitinated by the Kelch-like ECH-associated protein 1 (KEAP1)-Cullin 3 ubiquitin E3 ligase complex, which maintains the NRF2 protein at a low level by constitutive proteasomal degradation. However, KEAP1-mediated NRF2 degradation is blocked by oxidative and electrophilic stress. The stabilized NRF2 translocates to the nucleus to drive the transcription of cognate target genes, the protein products of which are involved in cellular antioxidant, detoxification, and metabolic pathways[2, 3]. The Cancer Genome Atlas (TCGA) catalogued genetic changes in the KEAP1-NRF2 axis in approximately 6.3% of all cancer patients[4]. These mutations phenotypically converge to constitutively activate NRF2. Otherwise, NRF2 hyperactivation occurs through the non-canonical pathway, where a subset of adaptor proteins (SQSTM1/p62, WTX, ATDC, PALB2, etc.) compete with NRF2 for binding to KEAP1, allowing NRF2 to evade KEAP1-mediated degradation[5].

Cytosolic dipeptidyl peptidase 9 (DPP9) and its close paralogue DPP8 are two members of the dipeptidyl peptidase IV enzyme family, characterized by the ability to cleave a dipeptide from the N-terminus of their substrates (preferentially post-proline)[6,7]. Although several strategic screenings for protease substrate

profiling have been performed, very few physiological substrates have been identified. The most well-known molecular function of DPP9 is endogenous inhibition of NLRP1 and CARD8 inflammasomes by directly binding to NLRP1 and CARD8, respectively[8]. Inhibiting DPP8/9 with Val-boroPro induces pro-caspase-1-dependent secretion of cytokines and pyroptotic cell death in monocytes and macrophages[9, 10]. In addition to the well-established function of DPP9 in the immune system, DPP9 also plays diverse roles in cell growth, migration and adhesion. Loss of DPP9 enzymatic activity is lethal in neonatal mice due to suckling defects[11]. Moreover, abnormal overexpression of DPP9 has been observed in multiple types of solid tumours, such as hepatocellular, ovarian, colorectal, breast carcinoma and non-small cell lung cancer, and is usually correlated with a poor prognosis and chemoresistance, indicating that DPP9 is a promising target for cancer therapy [12–16]. However, the pathophysiological functions of DPP9 in solid tumours are still poorly understood.

In this study, we revealed that DPP9 expression is oncogenically upregulated in ccRCC We showed that DPP9 promotes NRF2 pathway activation, suppresses ferroptosis, and causes sorafenib resistance in ccRCC cells by directly blocking KEAP1-mediated NRF2 degradation. Dysregulation of the KEAP1-NRF2-SLC7A11 axis partially contributes to DPP9 overexpression-induced ferroptosis suppression and sorafenib resistance.

2. Methods And Materials

2.1 Cell culture, transfection and antibodies

The human renal cell carcinoma (RCC) cell lines 786O and CCRFC1, as well as the human embryonic kidney cell line 293T, were obtained from the American Type Culture Collection (ATCC, Manassas, VA, USA). The 786O and CCRFC1 cells were maintained in RPMI-1640 media (Thermo Fisher Scientific, Waltham, MA, USA). The 293T cells were cultured in DMEM (Thermo). Media were supplemented with 10% (v/v) foetal bovine serum (Thermo) and 1% antibiotic (100 mg/ml streptomycin and 100 U/ml penicillin). All cells were grown and maintained at 37°C in a humidified incubator with 5% CO_2. The cell lines were routinely tested to exclude contamination by mycoplasma. Lipofectamine 2000 (Thermo) was used for transient transfection following the manufacturer's instructions. The antibodies used in this study are listed in **Supplementary Table 1**.

2.2 Protein complex purification

The DPP9-containing protein complexes were purified from 293T cells to detect DPP9-interacting proteins. Briefly, 293T cells were transiently transfected with the pCMV-FLAG-DPP9 plasmid. About 48 h after transfection, the 293T cells were washed twice with ice-cold phosphate-buffered saline (PBS) and lysed in ice-cold BC100 buffer (20 mM Tris-HCl, 0.2 mM EDTA, 100 mM NaCl, 20% glycerol, pH 7.9 0.2% Triton X-100) containing fresh protease inhibitors for 2 h. The whole-cell lysates were centrifuged at 12,000 rpm for 10 min, and the supernatants were carefully aspirated without disturbing the pellet and placed in new tubes. The DPP9-containing protein complexes were immunoprecipitated using anti-FLAG

antibody-conjugated M2 agarose (Sigma, St. Louis, MO, USA). The bound protein complexes were eluted using FLAG peptides. The eluates were resolved by sodium dodecyl sulphate-polyacrylamide gel electrophoresis (SDS-PAGE) on a 10% gradient gel (Bio-Rad, Hercules, CA, USA). After staining with Coomassie Blue (CB), the target gel bands were excised and subjected to mass spectrometry analysis.

2.3 CRISPR-Cas9-mediated gene knockout (KO) cell lines

To generate the KEAP1 and DPP9 KO cell lines, single-guided RNAs (sgRNAs) were cloned into the pX459 vector (Addgene, Watertown, MA, USA). Specific sgRNA sequences (listed in **Supplementary Table 2**) targeting KEAP1 or DPP9 were chosen using the optimized CRISPR design (http://crispr.mit.edu/). Plasmids expressing human Cas9 and KEAP1 sgRNA (plasmid KEAP1/pX459), and human Cas9 and DPP9 sgRNA (plasmid DPP9/pX459), were prepared by ligating the oligonucleotides into the pX459 *BbsI* site. To establish the KEAP1 and DPP9 KO cell lines, cells were seeded in a 10-cm dish and transfected with 10 μg of the KEAP1/pX459 and DPP9/pX459 plasmid, respectively, using Lipofectamine 2000. About 24 h after transfection, the cells were treated with 1 μg/ml puromycin for 3 days. Surviving cells were seeded in a 96-well plate at a limiting dilution to isolate the monoclonal cell lines. Single-cell clones stably expressing sgRNA were propagated and validated by Western blot (WB).

2.4 Cell viability assay

The viability of the ccRCC cells was detected using the Cell Counting Kit-8 (CCK-8; Dojindo, Tokyo, Japan) according to the manufacturer's instructions. Briefly, the cells were seeded in a 96-well plate at 2,000 cells/well. After the treatments, 10 μl of CCK-8 solution was added to the medium, followed by 2 h incubation at 37°C. Absorbance was measured at 450 nm using a microplate reader and normalized to the control. Cell viability was calculated using the results from three independent experiments.

2.5 ROS evaluation

Cells were plated in 6-well plates at 3×10^5 cells per well 24 h before analysis, and ROS levels were detected using the ROS Assay Kit (D6883; Sigma) according to the manufacturer's instructions. Briefly, following two washes with PBS, the cells were stained with 10 μM 2',7'dichlorodihydrofluorescein diacetate (DCFH-DA) and incubated at 37°C for 20 min. DCFH-DA is oxidized and converted into fluorescent 2', 7'-dichlorofluorescein by intracellular ROS. After washing three times with serum-free media to fully remove DCFH-DA that did not enter the cells, the cells were trypsinized, centrifuged and resuspended in PBS at a density of ~ 1×10^6 cells/ml. The fluorescence signals were detected using a flow cytometer (Beckman Coulter, Brea, CA, USA).

2.6 Liperfluo staining assay

To detect lipid peroxides, cells cultured in 6-cm dishes were exposed to Liperfluo (Dojindo) at a final concentration of 10 μM for 30 min at 37°C, according to the manufacturer's instructions. Following two washes with PBS, the cells were harvested and analysed using the flow cytometer.

2.7 Malondialdehyde (MDA) measurement

The relative MDA levels in cell lysates were measured using a Lipid Peroxidation Assay Kit (Colorimetric/Fluorometric) (#ab118970; Abcam, Cambridge, UK), according to the manufacturer's instructions. Briefly, thiobarbituric acid (TBA) was added to the supernatant, which reacted with MDA in the cell lysates to generate an MDA-TBA adduct for 1 h at 95°C. The absorbance of the MDA-TBA adduct was measured at 532 nm using a microplate reader and the result was normalized to that of the control. Each assay was performed in triplicate.

2.8 RNA isolation and quantitative real-time polymerase chain reaction (qRT-PCR)

Total RNA was extracted using TRIzol reagent (Tiangen, Beijing, China) according to the manufacturer's instructions. The amount and quality of total RNA were determined using a NanoDrop 2000 spectrophotometer (Thermo). Total RNA was reverse-transcribed into cDNA using a Superscript RT kit (TOYOBO, Dublin, OH, USA) with random primers, and qPCR amplification was carried out using the SYBR Green PCR Master Mix Kit (TOYOBO). Gene expression changes were normalized to the level of endogenous GAPDH and calculated using the 2^-ΔΔCT method. The primer sequences used for qRT-PCR are listed in **Supplementary Table 2**.

2.9 RNA sequencing (RNA-seq) and data analyses

A total of 500 ng of isolated RNA per sample was used as input material. Sequencing libraries were generated using a Ribo-off® rRNA Depletion Kit (Vazyme, Nanjing, China) and VAHTS® Universal V6 RNA-seq Library Prep Kit (Vazyme) for the Illumina platform following the manufacturer's instructions. Index codes were added to attribute the sequences to each sample. The libraries were sequenced on the Illumina platform, and 150 bp paired-end reads were generated.

RNA-seq raw data quality was assessed using FastQC (v0.11.9), and the adaptors were trimmed with Trim_Galore (version 0.6.6) before any data filtering criteria were applied. Reads were mapped onto the human reference genome (GRCh38.p13 assembly) using STAR software (v2.7.7a). The mapped reads were assembled into transcripts or genes using StringTie software (v2.1.4) and the genome annotation file (hg38_ucsc.annotated.gtf). The relative abundance of the transcripts was measured using normalized fragments per kilobase of transcript per million mapped reads (FPKM) metrics. Transcripts with an FPKM score > 1 were retained.

2.10 Glutathione (GSH) assay

The GSH level was evaluated using the Total Glutathione Assay Kit (S0052; Beyotime, Beijing, China), according to the manufacturer's instructions. Cultured 786O and CCRFC1 cells were trypsinized, deproteinized solution S was added, and the cells were vortexed. The cells were subjected to two quick freeze-thaw cycles using liquid nitrogen and a 37°C water bath. After 5 min in an ice bath, the cell lysates were centrifuged at 10,000 g for 10 min at 4°C. The supernatants were loaded into a 96-well plate to determine total GSH. Next, 150 μl of the total GSH detection working solution was added to each well and incubated for 5 min at room temperature (RT). A 50 μl aliquot of NADPH (0.5 mg/ml) solution was rapidly

added to the samples and the plate was mixed briefly on a shaker. The plates were incubated for 1 h at 37°C. Absorbance was measured at 412 nm using a microplate reader. Each assay was performed in triplicate.

2.11 GPX4 enzymatic assay

GPX4 enzymatic activity was detected using the Total Glutathione Peroxidase Assay Kit with NADPH (Beyotime), following the manufacturer's instructions. The cells were harvested and washed with cold PBS. Then, the cells were lysed with 200 μl assay buffer and centrifuged at 10,000 g for 15 min at 4°C. The supernatants were transferred to new tubes. Next, glutathione peroxidase detection buffer, GPX detection working buffer and the samples were loaded into a 96-well plate. The samples were mixed thoroughly and incubated at RT for 15 min. A 10 μl aliquot of peroxide solution (30 mM) was added to the wells, the plate was incubated at 25°C for 5 min, and the resulting colour was measured at 340 nm using a microplate reader. Each assay was performed in triplicate.

2.12 Immunofluorescence and confocal microscopy

Cells on round cover glasses were fixed for cell staining in 4% paraformaldehyde at RT for 15 min. The fixed cells were washed three times with PBS. The cells were permeabilised with 0.5% Triton X-100 in PBS for 10 min, and then in a blocking solution for 30 min at RT. The samples were stained with primary antibodies at 4°C overnight in antibody reaction buffer (PBS plus 1% BSA and 0.3% Triton X-100, pH 7.4). After washing three times with PBS (10 min each), fluorescence-labelled secondary antibodies were incubated for 30 min. The cells were washed three times (10 min each) after incubation with the secondary antibodies and then counterstained with DAPI (1 μg/ml) for 10 min at RT. The cells were subjected to confocal microscopy (LSM880; Carl Zeiss, Jena, Germany).

2.13 *In vivo* xenograft assay

Four–six-week-old BALB/c nude mice (weight 20–25 g) were obtained from Shanghai SLAC Laboratory Animal Co., Ltd. (Shanghai, China) for *in vivo* xenografts. Cultured 786O cells (5×10^6) were subcutaneously heterotransplanted into the right flank of all mice. The mice were maintained under specified conditions. When tumour volume increased to 50 mm^3, the sorafenib treatment groups were intravenously injected with sorafenib (10 mg/kg) every 2 days. Then, the tumour volume was calculated using the following formula: tumour volume = (long × $wide^2$) × 1/2, every 7 days. At the end of the experiment, the tumours were imaged, measured and weighed after euthanizing the mice. All procedures were performed with the approval of the Animal Care Committee of Fudan University.

2.14 Samples from ccRCC patients

A total of 207 patients with localized ccRCC, who underwent radical nephrectomy or partial nephrectomy between March 2005 and December 2009 at Fudan University Shanghai Cancer Centre (FUSCC), were included in this study. None of the patients received preoperative or postoperative adjuvant treatment. The patients underwent regular postoperative reviews and had long-term follow-up data. Seven pairs of fresh ccRCC tissues were obtained from October 2020 to December 2020 at FUSCC. The tumour tissues and adjacent non-cancerous tissues were collected and subjected to WB analysis. Twenty-six metastatic ccRCC specimens from patients who underwent cytoreductive surgery and sorafenib treatment between April 2006 and July 2009 were also included in the study. Patients with progressive disease during 1 year of the sorafenib treatment were defined as Sorafenib-resistant.

2.15 Immunohistochemistry (IHC) analysis

Tissue microarray (TMA) slides consisting of 207 localized and 26 metastatic ccRCC specimens were obtained from FUSCC patients.. Briefly, the TMA slides were deparaffinized, rehydrated, incubated with 3% H_2O_2 and blocked with goat serum. They were incubated with primary antibodies against DPP9 (ab62025; Abcam) or NRF2 (16396-1-AP; Proteintech, Rocky Hill, NJ, USA) overnight at 4°C. After three washes in PBS, the TMA slides were incubated with peroxidase-conjugated secondary antibody for 1 h at RT and stained with diaminobenzidine to detect the chromogens. All IHC staining intensities were assessed by two independent pathologists blinded to the clinical data. A 4-point scale (0, negative; 1, weak; 2, moderate; 3, intense) was used, and the quantity of immunostaining was classified (0, none; 1, 1–30%; 2, 31–60%; 3, > 60%). The total score was the product of the two scores. Patients were divided into high and low DPP9 expression groups according to the median IHC score.

2.16 Public database acquisition and analyzation

Pan-cancer gene expression analysis based on tumor and normal samples was derived from the TCGA and GTEx database, which is publicly accessible at http://gepia2.cancer-pku.cn/. Public databases (TCGA, Clinical Proteomic Tumour Analysis Consortium [CPTAC] and ICGC) were used to analyse the correlations of DPP9 expression with clinical risk factors and prognosis. The available RNA-seq data of 534 ccRCC patients from TCGA were obtained from the UCSC Xena website (https://xenabrowser.net/). The patients were divided into two groups for the survival analysis according to DPP9 expression, and high/low expression cut-off values were determined using X-tile software. We acquired quantitative proteomics data for 110 ccRCC patients from the CPTAC database (proteomics.cancer.gov/programs/cptac). We also obtained RNA-seq data of 91 ccRCC patients from ICGC database (https://icgc.org/). The DPP9 protein level of normal and tumor tissues was also analyzed from a large-scale proteomic analysis of 213 ccRCC in a Chinese population[17].

2.17 Statistical analysis

Statistical analyses were performed using GraphPad Prism software (GraphPad Software, Inc., La Jolla, CA, USA). Data are presented as mean ± SD for experiments performed independently at least three times. Differences between the two groups were analysed by two-way analysis of variance. Survival analysis was performed using the Kaplan–Meier method and log-rank test. A p-value < 0.05 was considered significant. *p < 0.05; **p < 0.01; ***p < 0.001.

3. Results

3.1 DPP9 expression is upregulated in ccRCC and correlates with a poor prognosis in ccRCC patients

Previous studies indicated that DPP9 promotes tumorigenesis in several types of cancer[13–16.18–20]. However, it is unknown whether DPP9 is aberrantly expressed in ccRCC, the most frequent histological subtype of RCC. To address this issue, we investigated the expression pattern of DPP9 in ccRCC by analysing publicly available TCGA ccRCC dataset. As shown in Fig. 1A, DPP9 mRNA expression was markedly upregulated in ccRCC tissues compared with normal kidney tissues. In contrast, DPP9 expression was moderately altered in kidney chromophobe and renal papillary cell carcinoma, which are both relatively uncommon histological subtypes of RCC. The upregulation of DPP9 in ccRCC was also validated in the ICGC ccRCC cohort (**Supplementary Fig. 1A**). The CPTAC dataset showed that DPP9 was most markedly upregulated at the protein level among the tumour types examined (Fig. 1B). A similar trend was observed in a large-scale proteomic analysis of 213 ccRCC specimens from a Chinese FUSCC cohort (**Supplementary Fig. 1B**)[17].

Analysis of the TCGA ccRCC dataset revealed that DPP9 mRNA expression was positively correlated with several clinical parameters, including T stage (Fig. 1C), TNM stage (Fig. 1D), and pathological grade (Fig. 1E). Positive correlations between DPP9 protein expression and advanced TNM stage/pathological grade were independently validated by analysing the CPTAC dataset (Figs. 1F, G). We confirmed that DPP9 protein expression was upregulated in five of seven fresh ccRCC tissues compared with adjacent non-cancerous tissues, as assessed by WB analysis (Figs. 1H, I). We further evaluated DPP9 protein expression in ccRCC by IHC analysis of a TMA consisting of 207 ccRCC and adjacent non-cancerous tissues from the FUSCC cohort. As shown in Fig. 1J, DPP9 staining intensity in tumour tissues was classified as negative, low, or high. Strong upregulation of the DPP9 protein was observed in ccRCC tissues compared to adjacent non-cancerous tissues (Fig. 1K). Furthermore, survival analysis indicated that high DPP9 expression was significantly correlated with shorter overall survival in the TCGA and FUSCC ccRCC cohorts (Figs. 1L, M). Taken together, our results indicate that DPP9 expression aberrantly increased in ccRCC and was correlated with a poor prognosis in ccRCC patients.

3.2 Identification of KEAP1 as a DPP9-interacting protein

To identify potential molecular mediators of DPP9's oncogenic function, we isolated DPP9 protein complexes from 293T cells overexpressing FLAG-DPP9 and determined the proteins present in the

complexes by mass spectrometry (Fig. 2A). KEAP1 was present in the complexes and ranked with high confidence in the interaction hit list. Considering the pivotal roles of the KEAP1-NRF2 pathway in cancer, we conducted further analyses to determine the pathophysiological significance of the DPP9–KEAP1 interaction.

We first verified the binding of KEAP1 to DPP9 in co-immunoprecipitation assays by overexpressing KEAP1 and DPP9 (Figs. 2B, C). Endogenous interaction between DPP9 and KEAP1 was observed in ccRCC 786O cells (Figs. 2D, E). Next, we determined the protein sequence mediated the mutual interaction between KEAP1 and DPP9. Previous studies have demonstrated that KEAP1-associated proteins (e.g. Nrf2, IKKβ, and PGAM5) contain consensus ESGE, ETGE and/or DLG motifs that are responsible for binding to the KELCH domain of KEAP1[2, 3]. DPP9 contained a perfectly matched ETGE and ESGE motif, but no DLG motif was found. Notably, the ESGE motif was highly conserved among different species, from humans to zebrafish. In contrast, the ETGE motif was not conserved, and was not present in the DPP9 proteins of frog or zebrafish (Fig. 2F). Deletion of the ESGE motif, but not the ETGE motif, completely abolished the KEAP1-DPP9 interaction (Fig. 2G). KEAP1 contained a CUL3-binding BTB-BACK domain and the KELCH domain responsible for binding to substrates, including NRF2 (Fig. 2H). The KEAP1 KELCH domain, but not the BTB or IVR domain, mediated its interaction with DPP9 (Fig. 2I). Finally, we demonstrated defective binding of cancer-derived KEAP1 mutants in the KLECH domain to DPP9, analogous to the KEAP1-NRF2 interaction (Fig. 2J). Taken together, our results indicate that DPP9 interacts with KEAP1 via the ESGE motif.

3.3 DPP9 promotes NRF2 stabilisation and nuclear accumulation by competitively binding to KEAP1

After validating the interaction between KEAP1 and DPP9, we explored whether KEAP1 targets DPP9 for ubiquitin-dependent degradation, similar to its authentic substrate, NRF2. However, KEAP1 overexpression did not alter the protein level of ectopically co-expressed DPP9 (Fig. 3A). To examine the effect of KEAP1 on endogenous DPP9, we generated Tet-on-inducible 786O cells that conditionally express FLAG-KEAP1. The induction of exogenous KEAP1 led to a time-dependent reduction in the NRF2 protein level, whereas the DPP9 protein level remained unchanged (Fig. 3B). Furthermore, depleting KEAP1 by CRISPR/Cas9-mediated KO in 293T and 786O cells did not change the DPP9 protein level, but markedly upregulated the NRF2 protein level (Fig. 3C).

Previous studies revealed that the ETGE motif-harbouring KEAP1-interacting proteins, such as SQSTM1, iASPP, and PALB2 sequester KEAP1, leading to increased stability and activation of NRF2[21–23]. We investigated whether DPP9 affects the NRF2 protein level through its interaction with KEAP1. Depleting DPP9 with siRNAs in 293T cells downregulated the NRF2 protein level (Fig. 3D). DPP9 KO in 786O cells and another RCC cell line, CCRFC1, led to a marked decrease in NRF2, HMOX1 and SLC7A11 protein levels (Fig. 3E). HMOX1 and SLC7A11 are two representative transcriptional targets of NRF2[24]. DPP9 KO shortened the half-life of NRF2 in 786O cells (Figs. 3F, G), whereas DPP9 overexpression prolonged the half-life of NRF2 (**Supplementary Figs. 2A, B**), indicating that DPP9 positively regulates NRF2 protein

stability. Overexpression of DPP9-WT, but not the ΔESGE mutant, increased the protein levels of NRF2, HMOX1, and SLC7A11 in a dose-dependent manner (Fig. 3H). As DPP9 is an intracellular prolyl peptidase, we generated the catalytically dead mutant DPP9-S759A to evaluate whether the NRF2 protein level was affected by DPP9 enzymatic activity. However, reintroducing the DPP-S759A mutant into DPP9-KO cells increased NRF2 protein to a level similar to that of DPP9-WT (Fig. 3I). Treating 786O cells with a potent DPP9 enzymatic inhibitor 1G244 did not affect the NRF2 protein level, indicating that DPP9 peptidase activity is dispensable for regulating NRF2 (**Supplementary Fig. 2C**).

We evaluated the role of DPP9 in protecting NRF2 from KEAP1-mediated degradation. DPP9-WT, but not the ΔESGE mutant, reduced the KEAP1-NRF2 binding affinity and KEAP1-mediated NRF2 ubiquitination (Figs. 3J, K). As the DPP9-KEAP1 interaction enhanced the stability of NRF2, human tumours overexpressing DPP9 may upregulate the NRF2 protein level. Indeed, the IHC analysis showed that their expression was positively correlated in FUSCC ccRCC cohort (Figs. 3L, M). Taken together, these results indicate that DPP9 stabilizes NRF2 in ccRCC cells by competitively binding to KEAP1.

3.4 DPP9 enhances the transcriptional outputs of the NRF2 pathway

To evaluate the outcome of DPP9-mediated NRF2 regulation, we investigated the global transcriptomic changes induced by DPP9 KO in 786O cells by RNA-seq (Fig. 4A). Among the 322 reported transcriptional targets of NRF2, multiple genes were significantly downregulated in DPP9 KO cells, including SLC7A11, HMOX1, AIFM2, TXNRD1 and TXN[25, 26]. (Fig. 4B, **Supplementary Table 3**). The decrease in HMOX1 and SLC7A11 mRNA levels was confirmed by qRT-PCR (Fig. 4C). Conversely, overexpression of DPP9-WT, but not the ΔESGE mutant, increased the HMOX1 and SLC7A11 mRNA levels (Fig. 4D). By analysing the RNA-seq dataset of the TCGA ccRCC cohort, we found that the mRNA expression levels of DPP9 and several NRF2 transcriptional targets (SLC7A11, HMOX1, TXNRD1, and AIFM2) were positively correlated (Figs. 4E, F). Taken together, these results indicate that DPP9 positively regulates the transcriptional outputs of the NRF2 pathway.

3.5 DPP9 regulates cellular ROS levels in a KEAP1-binding dependent manner

NRF2 is a central hub that neutralizes ROS and restores the cellular redox balance. As DPP9 promotes the stability of the NRF2 protein, we explored whether DPP9 affects redox balance in ccRCC cells. As a result, DPP9 KO led to significant ROS accumulation. Reintroducing DPP9-WT into DPP9 KO 786O cells reversed this effect, whereas reintroducing the DPP9-ΔESGE mutant failed to do so (Figs. 5A, B). Exposure to hydrogen peroxide (H_2O_2) is widely used to trigger oxidative stress in cellular models. Much weaker nuclear translocation of NRF2 was observed in DPP9 KO 786O than parental cells after the H_2O_2 treatment (Fig. 5C). Stronger binding between KEAP1 and DPP9 was also observed after the H_2O_2 treatment (Fig. 5D). Moreover, the H_2O_2 treatment triggered much weaker induction of NRF2, HOMX1, and SLC7A11 in DPP9 KO 786O cells than parental cells. Reintroducing DPP9-WT into DPP9 KO 786O cells

reversed these effects, but the ΔESGE mutant did not (Figs. 5E, F). Consistent with their effects on the ROS level, DPP9 KO 786O and CCRFC1 cells were more sensitive to H_2O_2-induced cell death than parental cells. Reintroducing DPP9-WT into DPP9 KO 786O cells reversed these effects, but the DPP9-ΔESGE mutant did not (Figs. 5G, H). Taken together, these results indicate that overexpressing DPP9 reduces cellular ROS levels, thereby leading to resistance to oxidative stress-induced cell death in ccRCC cells.

3.6 DPP9 overexpression contributes to ferroptosis suppression in a SLC7A11-dependent manner

The aforementioned results show that overexpressing DPP9 induced the upregulation of SLC7A11, which imports cystine for GSH biosynthesis, thereby protecting cells from oxidative stress and ferroptosis; this is a regulated form of non-apoptotic cell death driven by the accumulation of lipid-based ROS, particularly lipid hydroperoxides[27, 28]. Gene set enrichment analysis (GSEA) of the RNA-seq data indicated that the DPP9 KO-affected genes were enriched in the ferroptosis process (Fig. 6A, **Supplementary Table 4**). Electron microscopic analysis showed that DPP9 KO cells had prominent swollen mitochondria and increased mitochondrial membrane density, and lacked mitochondrial cristae, which are typical morphological changes during ferroptosis (Fig. 6B). We used Liperfluo staining to monitor lipid peroxidation during ferroptosis and found that the Liperfluo signals were more prominent in DPP9 KO 786O cells; this was reversed by reintroducing DPP9-WT, but not the ΔESGE mutant (Fig. 6C).

The classic ferroptotic inducer erastin elicited more cell death in DPP9 KO 786O cells than parental cells; this effect was largely eliminated by co-treatment with ferrostatin (Ferr-1) or deferoxamine (DFO), which are selective inhibitors of ferroptosis. Reintroducing DPP9-WT into DPP9 KO 786O cells reversed their vulnerability to sorafenib, but the DPP9-ΔESGE mutant did not (Fig. 6D). Furthermore, overexpression of DPP9-WT, but not the ΔESGE mutant, resulted in resistance of 786O cells to erastin-induced cell death (Fig. 6E). To further delineate whether DPP9 KO promotes ferroptosis by inhibiting SLC7A11 expression, we stably overexpressed SLC7A11 in DPP9 KO 786O cells. The restoration of SLC7A11 expression in DPP9 KO cells reversed erastin-induced cell death (Fig. 6F). Moreover, restoring SLC7A11 expression largely reversed DPP9 KO-induced changes in GPX4 enzymatic activity (Fig. 6G, **Supplementary Fig. 3A**), and the levels of MDA (Fig. 6H, **Supplementary Fig. 3B**) and cellular GSH (Fig. 6I, **Supplementary Fig. 3C**). Taken together, these results indicate that DPP9 suppresses ferroptosis in a SLC7A11-dependent manner.

3.7 DPP9 overexpression contributes to resistance to sorafenib in ccRCC

Sorafenib is a multikinase inhibitor used to treat advanced ccRCC and hepatocellular carcinoma (HCC)[29]. It was first proposed to act as a potent inducer of ferroptosis by inhibiting SLC7A11 activity[30]. Therefore, we suspected that aberrant overexpression of DPP9 in ccRCC may cause intrinsic sorafenib resistance by suppressing ferroptosis. We found that overexpressing DPP9 in 786O and CCRFC1 cells suppressed sorafenib-induced cell death (Fig. 7A). The sorafenib treatment elicited more cell death in DPP9 KO 786O than parental cells, and this effect was largely eliminated by co-treatment with Ferr-1 or

DFO. Reintroducing DPP9-WT into DPP9 KO 786O cells reversed their vulnerability to sorafenib, but the DPP9-ΔESGE mutant did not (Fig. 7B). Furthermore, overexpression of DPP9-WT, but not the ΔESGE mutant, resulted in resistance of 786O cells to sorafenib (Fig. 7C).

We examined whether DPP9 induces sorafenib resistance in a xenograft tumour model. DPP9 KO markedly suppressed 786O tumour growth and potentiated sorafenib-induced tumour suppression (Figs. 7D–F). Analysis of the IHC data from the sorafenib treatment cohort showed that higher DPP9 overexpression was correlated with sorafenib resistance in ccRCC (Fig. 7G). Taken together, these results indicate that overexpressing DPP9 contributed to sorafenib resistance in ccRCC.

4. Discussion

Hyperactivation of the NRF2 pathway confers cancer cell resistance to anti-cancer drugs and oxidative stress, and directs cancer cells toward metabolic rewiring of tumours (which promotes tumorigenesis and progression). Therefore, targeting the NRF2 pathway is a promising therapeutic strategy for various cancers, including ccRCC[31]. The present study provides evidence that DPP9 binds to and sequesters KEAP1, upregulates the NRF2 protein level and transcriptional outputs, reduces cellular ROS levels, and suppresses ferroptosis, thereby driving ccRCC tumorigeneses and sorafenib resistance.

Mutations in KEAP1, CUL3 and NFE2L2 have been reported in a relatively small fraction (6.6%) of ccRCC cases[32]. However, several studies have demonstrated a generally strong effect of NRF2 hyperactivation in ccRCC, indicating that other mechanisms may regulate the NRF2 pathway. In addition to direct canonical regulation of the NRF2 pathway by KEAP1, non-canonical regulation of the NRF2 pathway by proteins (p62/SQSTM1, PLAB2, WTX, ADTC and DPP3) can disrupt the KEAP1-NRF2 interaction, as reported in several cancer-related studies [24,33–36]. Most of these proteins harbour the “ETGE” or “ESGE” motif, which mediates competitive binding with KEAP1 from NRF2. For example, ATDC interacts with KEAP1 to drive NRF2-mediated tumorigenesis and chemoresistance in pancreatic cancer[35]. DPP3 abrogates KEAP1-mediated NRF2 degradation to support breast cancer survival under oxidative stress[36]. ADTC and DPP3 are overexpressed in pancreatic and breast cancers, respectively, and their expression is correlated with poor survival[35, 37]. Similarly, DPP9 binds to KEAP1 through an ESGE motif that competes with the ETGE motif, thereby stabilising NRF2 in ccRCC. In the present study, we established that the ESGE motif-harboring protein DPP9 is a novel non-canonical regulator of the NRF2 pathway (Fig. 8). Importantly, DPP9 is overexpressed in multiple types of cancer. We analysed the RNA sequencing dataset of TCGA cancer cohorts deposited in the GEPIA2 database (http://gepia2.cancer-pku.cn/#general) and found that DPP9, but no other reported non-canonical regulators of the NRF2 pathway, was significantly overexpressed in ccRCC (data not shown), indicating that DPP9 may play a substantial role in NRF2 hyperactivation in ccRCC. Moreover, we demonstrated that DPP9 peptidase activity was not required for regulation of the KEAP1-NRF2 pathway, indicating the diverse roles of DPP9 in cellular processes. We also suggest that blocking the interaction between DPP9 and KEAP1 using small molecules is a possible therapeutic strategy to reduce activation of the NRF2 protein and pathway in ccRCC.

Sorafenib is an orally administered multi-target kinase inhibitor that inhibits certain receptor tyrosine kinases (RTKs), including VEGFR1/2, PDGFR, KIT, FLT3, RET and CSF1R[38]. Studies have revealed that SLC7A11, a key mediator of ferroptosis, is inhibited by sorafenib[39]. Sorafenib is the first targeted drug approved by the FDA for treating metastatic ccRCC, which paved the way for the approval of other targeted agents and revolutionized the treatment of ccRCC[40]. Unfortunately, the increasing prevalence of sorafenib resistance has become a major obstacle to sorafenib therapy for patients with ccRCC. Approximately 22% of ccRCC patients are intrinsically resistant to sorafenib, and most (if not all) of the remaining patients exhibit sorafenib resistance and tumour progression after 6–15 months of therapy[38]. Underlying mechanisms of sorafenib resistance in ccRCC have been proposed, including altered expression of efflux and influx transporters, the epithelial-mesenchymal transition, self-renewal of cancer stem cells, changes in the tumour microenvironment and redox reprogramming[38]. Fully elucidating the molecular mechanism would help predict and monitor the clinical efficacy of sorafenib in patients with ccRCC. The increase of NRF2 activity in cases of drug resistance is well established. The role of the KEAP1-NRF2 pathway in sorafenib resistance has attracted considerable attention. Two CRISPR/Cas9 genome-wide screenings identified KEAP1 as a “sorafenib sensitivity gene” in HCC[41, 42]. Gao et al. showed that the protein levels of NRF2 and its targets are markedly induced in sorafenib-resistant HCC cells, and the malignant phenotypes of the cells are negated following NRF2 KO. YAP/TAZ and ATF4 drive sorafenib resistance by upregulating SLC7A11[41]. The results of this study suggest that overexpression of DPP9 in ccRCC likely contributes to intrinsic sorafenib resistance by upregulating the NRF2-SLC7A11 axis. This finding may help guide sorafenib use in ccRCC treatment.

Declarations

Authors’ contributions

KC, YC, and XZ performed most of the experiments and contributed to writing the manuscript. WZ and BZ performed part of the experiments. CW, DY and FX conceived the study, participated in its design and coordination and helped draft the manuscript. BD collected clinical samples and analyzed part of the data. All the authors have read and approved the final manuscript.

Declaration of competing interests

The authors declare no potential conflicts of interest.

Ethics approval

This study was approved by the Research Ethics Committee of Shanghai Cancer Center, Fudan University. Informed consent for the use of clinical data was obtained from all the patients recruited in this study. The study protocol conforms to the ethics guideline of the Declaration of Helsinki (as revised in Fortaleza, Brazil, October 2013).

Acknowledgements

This work was supported in part by the National Natural Science Foundation of China (No. 91957125, 81972396, and 81672558 to CJ.W. No.81902614 to KC. No.82172703 to BD), and the Natural Science Foundation of Shanghai (22ZR1406600 to CJ.W.), and Science and Technology Research Program of Shanghai (No. 9DZ2282100). This study was also partly supported by the Shanghai Sailing Program (19YF1408600 to KC). This study was also partly supported by a grant from the Natural Science Foundation of Science and Technology Commission of Shanghai Municipality (20ZR1412300).

References

1. Murphy MP, Bayir H, Belousov V, Chang CJ, Davies KJA, Davies MJ, et al. Guidelines for measuring reactive oxygen species and oxidative damage in cells and in vivo. Nat Metab. 2022 Jun;4(6):651–662.
2. Kobayashi A, Kang MI, Okawa H, Ohtsuji M, Zenke Y, Chiba T, et al. Oxidative stress sensor Keap1 functions as an adaptor for Cul3-based E3 ligase to regulate proteasomal degradation of Nrf2. Mol Cell Biol 2004; 24: 7130–7139.
3. Zhang DD, Lo SC, Cross JV, Templeton DJ, Hannink M. Keap1 is a redox-regulated substrate adaptor protein for a Cul3-dependent ubiquitin ligase complex. Mol Cell Biol 2004; 24: 10941–10953.
4. Cloer EW, Goldfarb D, Schrank TP, Weissman BE, Major MB. NRF2 Activation in Cancer: From DNA to Protein. Cancer Res. 2019 Mar 1;79(5):889–898.
5. Silva-Islas CA, Maldonado PD. Canonical and non-canonical mechanisms of Nrf2 activation. Pharmacol Res. 2018 Aug;134:92–99.
6. Zhang H, Chen Y, Keane FM, Gorrell MD. Advances in understanding the expression and function of dipeptidyl peptidase 8 and 9. Mol Cancer Res. 2013 Dec;11(12):1487–96.
7. Wilson CH, Zhang HE, Gorrell MD, Abbott CA. Dipeptidyl peptidase 9 substrates and their discovery: current progress and the application of mass spectrometry-based approaches. Biol Chem. 2016 Sep 1;397(9):837 – 56.
8. Taabazuing CY, Griswold AR, Bachovchin DA. The NLRP1 and CARD8 inflammasomes. Immunol Rev. 2020 Sep;297(1):13–25.
9. Adams S, Miller GT, Jesson MI, Watanabe T, Jones B, Wallner BP. PT-100, a small molecule dipeptidyl peptidase inhibitor, has potent antitumor effects and augments antibody-mediated cytotoxicity via a novel immune mechanism. Cancer Res. 2004 Aug 1;64(15):5471-80.
10. Walsh MP, Duncan B, Larabee S, Krauss A, Davis JP, Cui Y, et al. Val-boroPro accelerates T cell priming via modulation of dendritic cell trafficking resulting in complete regression of established murine tumors. PLoS One. 2013;8(3):e58860.
11. Gall MG, Chen Y, Vieira de Ribeiro AJ, Zhang H, Bailey CG, Spielman DS, et al. Targeted inactivation of dipeptidyl peptidase 9 enzymatic activity causes mouse neonate lethality. PLoS One. 2013 Nov 6;8(11):e78378.

12. Henderson JM, Xiang MSW, Huang JC, Wetzel S, Jiang L, Lai JH, et al. Dipeptidyl Peptidase Inhibition Enhances CD8 T Cell Recruitment and Activates Intrahepatic Inflammasome in a Murine Model of Hepatocellular Carcinoma. Cancers (Basel). 2021 Nov 1;13(21):5495.
13. Smebye ML, Agostini A, Johannessen B, Thorsen J, Davidson B, Tropé CG, Heim S, Skotheim RI, Micci F. Involvement of DPP9 in gene fusions in serous ovarian carcinoma. BMC Cancer. 2017 Sep 11;17(1):642.
14. Wilson CH, Abbott CA. Expression profiling of dipeptidyl peptidase 8 and 9 in breast and ovarian carcinoma cell lines. Int J Oncol. 2012 Sep;41(3):919–32.
15. Tang Z, Li J, Shen Q, Feng J, Liu H, Wang W, et al. Contribution of upregulated dipeptidyl peptidase 9 (DPP9) in promoting tumoregenicity, metastasis and the prediction of poor prognosis in non-small cell lung cancer (NSCLC). Int J Cancer. 2017 Apr 1;140(7):1620–1632.
16. Saso K, Miyoshi N, Fujino S, Sasaki M, Yasui M, Ohue M, et al. Dipeptidyl Peptidase 9 Increases Chemoresistance and is an Indicator of Poor Prognosis in Colorectal Cancer. Ann Surg Oncol. 2020 Oct;27(11):4337–4347.
17. Qu Y, Feng J, Wu X, Bai L, Xu W, Zhu L, et al. A proteogenomic analysis of clear cell renal cell carcinoma in a Chinese population. Nat Commun. 2022 Apr 19;13(1):2052.
18. Brunetti M, Holth A, Panagopoulos I, Staff AC, Micci F, Davidson B. Expression and clinical role of the dipeptidyl peptidases DPP8 and DPP9 in ovarian carcinoma. Virchows Arch. 2019 Feb;474(2):177–185.
19. Bolgi O, Silva-Garcia M, Ross B, Pilla E, Kari V, Killisch M, et al. Dipeptidyl peptidase 9 triggers BRCA2 degradation and promotes DNA damage repair. EMBO Rep. 2022 Aug 1:e54136.
20. Johnson DC, Taabazuing CY, Okondo MC, Chui AJ, Rao SD, Brown FC, et al. DPP8/DPP9 inhibitor-induced pyroptosis for treatment of acute myeloid leukemia. Nat Med. 2018 Aug;24(8):1151–1156.
21. Ge W, Zhao K, Wang X, Li H, Yu M, He M, et al. iASPP Is an Antioxidative Factor and Drives Cancer Growth and Drug Resistance by Competing with Nrf2 for Keap1 Binding. Cancer Cell. 2017 Nov 13;32(5):561–573.e6.
22. Gao K, Shi Q, Liu Y, Wang C. Enhanced autophagy and NFE2L2/NRF2 pathway activation in SPOP mutation-driven prostate cancer. Autophagy. 2022 Aug;18(8):2013–2015.
23. Ma J, Cai H, Wu T, Sobhian B, Huo Y, Alcivar A, et al. PALB2 interacts with KEAP1 to promote NRF2 nuclear accumulation and function. Mol Cell Biol. 2012 Apr;32(8):1506–17.
24. Rojo de la Vega M, Chapman E, Zhang DD. NRF2 and the Hallmarks of Cancer. Cancer Cell. 2018 Jul 9;34(1):21–43.
25. Romero R, Sayin VI, Davidson SM, Bauer MR, Singh SX, LeBoeuf SE, et al. Keap1 loss promotes Kras-driven lung cancer and results in dependence on glutaminolysis. Nat Med. 2017 Nov;23(11):1362–1368.
26. Koppula P, Lei G, Zhang Y, Yan Y, Mao C, Kondiparthi L, et al. A targetable CoQ-FSP1 axis drives ferroptosis- and radiation-resistance in KEAP1 inactive lung cancers. Nat Commun. 2022 Apr 22;13(1):2206.

27. Stockwell BR, Jiang X, Gu W. Emerging Mechanisms and Disease Relevance of Ferroptosis. Trends Cell Biol. 2020 Jun;30(6):478–490.
28. Doll S, Freitas FP, Shah R, Aldrovandi M, da Silva MC, Ingold I, et al. FSP1 is a glutathione-independent ferroptosis suppressor. Nature. 2019 Nov;575(7784):693–698.
29. Llovet JM, Ricci S, Mazzaferro V, Hilgard P, Gane E, Blanc JF, de Oliveira AC, Santoro A, et al. Sorafenib in advanced hepatocellular carcinoma. N Engl J Med. 2008 Jul 24;359(4):378–90.
30. Dixon SJ, Patel DN, Welsch M, Skouta R, Lee ED, Hayano M, et al. Pharmacological inhibition of cystine-glutamate exchange induces endoplasmic reticulum stress and ferroptosis. Elife. 2014 May 20;3:e02523.
31. Kabel AM, Atef A, Estfanous RS. Ameliorative potential of sitagliptin and/or resveratrol on experimentally-induced clear cell renal cell carcinoma. Biomed Pharmacother. 2018 Jan;97:667–674.
32. Clerici S, Boletta A. Role of the KEAP1-NRF2 Axis in Renal Cell Carcinoma. Cancers (Basel). 2020 Nov 20;12(11):3458.
33. Komatsu M, Kurokawa H, Waguri S, Taguchi K, Kobayashi A, Ichimura Y, et al. The selective autophagy substrate p62 activates the stress responsive transcription factor Nrf2 through inactivation of Keap1. Nat Cell Biol. 2010 Mar;12(3):213–23.
34. Camp ND, James RG, Dawson DW, Yan F, Davison JM, Houck SA, et al. Wilms tumor gene on X chromosome (WTX) inhibits degradation of NRF2 protein through competitive binding to KEAP1 protein. J Biol Chem. 2012 Feb 24;287(9):6539–50.
35. Purohit V, Wang L, Yang H, Li J, Ney GM, Gumkowski ER, et al. ATDC binds to KEAP1 to drive NRF2-mediated tumorigenesis and chemoresistance in pancreatic cancer. Genes Dev. 2021 Feb 1;35(3–4):218–233.
36. Hast BE, Goldfarb D, Mulvaney KM, Hast MA, Siesser PF, Yan F, et al. Proteomic analysis of ubiquitin ligase KEAP1 reveals associated proteins that inhibit NRF2 ubiquitination. Cancer Res. 2013 Apr 1;73(7):2199 – 210.
37. Lu K, Alcivar AL, Ma J, Foo TK, Zywea S, Mahdi A, et al. NRF2 Induction Supporting Breast Cancer Cell Survival Is Enabled by Oxidative Stress-Induced DPP3-KEAP1 Interaction. Cancer Res. 2017 Jun 1;77(11):2881–2892.
38. He Y, Luo Y, Huang L, Zhang D, Wang X, Ji J, et al. New frontiers against sorafenib resistance in renal cell carcinoma: From molecular mechanisms to predictive biomarkers. Pharmacol Res. 2021 Aug;170:105732.
39. Koppula P, Zhuang L, Gan B. Cystine transporter SLC7A11/xCT in cancer: ferroptosis, nutrient dependency, and cancer therapy. Protein Cell. 2021 Aug;12(8):599–620.
40. Escudier B, Eisen T, Stadler WM, Szczylik C, Oudard S, Siebels M, et al. Sorafenib in advanced clear-cell renal-cell carcinoma. N Engl J Med. 2007 Jan 11;356(2):125–34.
41. Gao R, Kalathur RKR, Coto-Llerena M, Ercan C, Buechel D, Shuang S, et al. YAP/TAZ and ATF4 drive resistance to Sorafenib in hepatocellular carcinoma by preventing ferroptosis. EMBO Mol Med. 2021 Dec 7;13(12):e14351.

42. Zheng A, Chevalier N, Calderoni M, Dubuis G, Dormond O, Ziros PG, et al. CRISPR/Cas9 genome-wide screening identifies KEAP1 as a sorafenib, lenvatinib, and regorafenib sensitivity gene in hepatocellular carcinoma. Oncotarget. 2019 Dec 17;10(66):7058–7070.

Figures

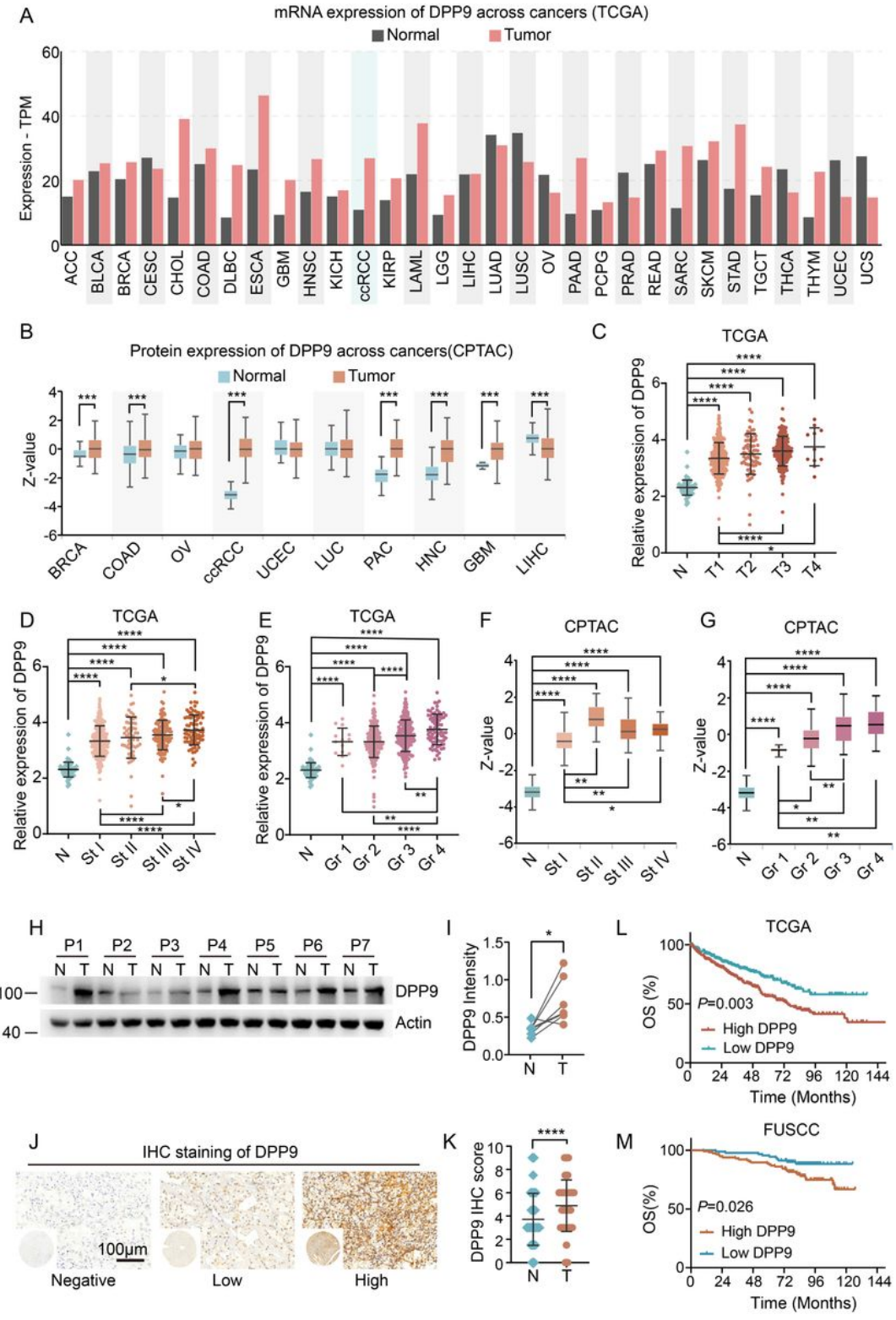

Figure 1

The expression of DPP9 in ccRCC and its relationship with the prognosis of ccRCC patients.

(**A**) DPP9 mRNA levels in normal and tumour tissues from the TCGA cohort.

(**B**) DPP9 protein levels of normal and different tumour tissues of patients in the CPTAC cohort.

(**C**–**E**) Relationship between DPP9 mRNA expression and T stage (**C**), clinical TNM stage (**D**), and pathological grade (**E**) in patients in the TCGA ccRCC cohort.

(**F**, **G**) Relationship between DPP9 protein expression and clinical TNM stage (**F**) and pathological grade (**G**)in ccRCC patients in the CPTAC ccRCC cohort.

(**H**, **I**) WB detected DPP9 protein expression in ccRCC tissues (T) and adjacent noncancerous tissues (N) from the FUSCC ccRCC cohort (**H**). The protein level of DPP9 relative to that of actin was measured using ImageJ (NIH, Bethesda, MD, USA) (**I**).

(**J**, **K**) IHC analysis of the DPP9 protein in ccRCC TMA (n = 207). Representative staining results for DPP9, classified as negative, low or high expression. Scale bar, 100 μm. (**J**). Results of a quantification analysis (**K**).

(**L**) Kaplan–Meier survival plots of OS according to DPP9 mRNA expression in ccRCC specimens from the TCGA ccRCC cohort.

(**M)** Kaplan–Meier survival plots of OS according to DPP9 protein expression in ccRCC specimens from the FUSCC ccRCC cohort.

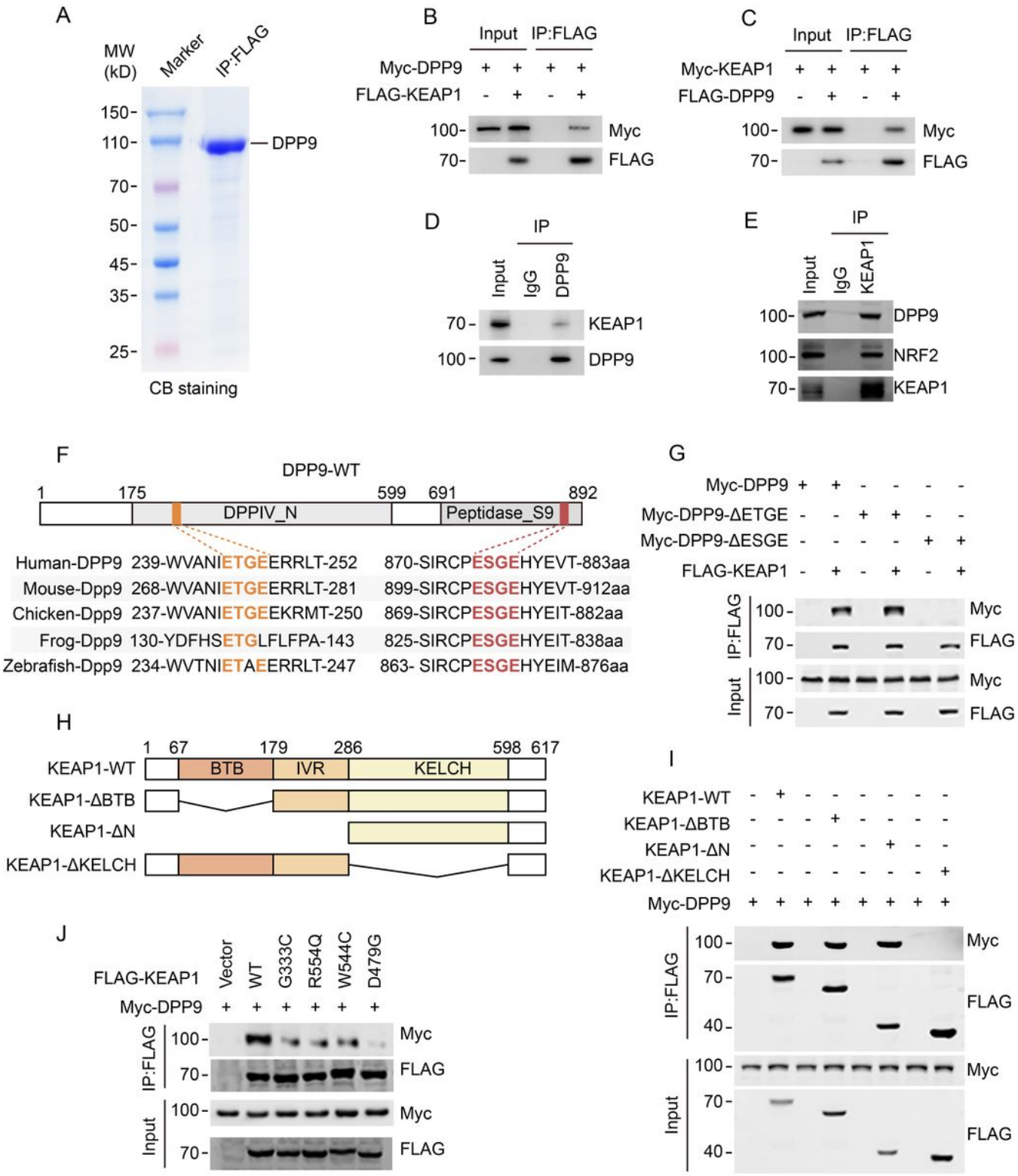

Figure 2

Identifying KEAP1 as a DPP9-interacting protein.

(**A**) Isolation of DPP9-containing protein complexes from 293T cells overexpressing FLAG-DPP9. The derived proteins were separated by SDS-PAGE and visualized by CB staining.

(**B**, **C**) The indicated plasmids were transiently transfected into 293T cells. Whole-cell lysates were harvested and immunoprecipitated with anti-FLAG antibodies. The input and immunoprecipitates were analysed by WB with the indicated antibodies.

(**D**, **E**) Whole 786O cell lysates were harvested and immunoprecipitated with anti-DPP9 (**D**) or anti-KEAP1 (**E**) antibodies. The input and immunoprecipitates were analysed by WB with the indicated antibodies.

(**F**) The protein sequence alignment of the ETGE and ESGE motifs in DPP9 from humans to zebrafish.

(**G**) The indicated plasmids were transfected into 786O cells. Whole-cell lysates were harvested and immunoprecipitated with the anti-FLAG antibody. The input and immunoprecipitates were analysed by WB with the indicated antibodies.

(**H**) Schematic of the different KEAP1 motifs (upper panel) and three schematics of recombinant plasmids expressing different truncated KEAP1 mutants.

(**I**) The indicated plasmids were transfected into 786O cells. Whole-cell lysates were harvested and immunoprecipitated with the anti-FLAG antibody. The input and immunoprecipitates were analysed by WB with the indicated antibodies.

(**J**) The indicated plasmids were transfected into 786O cells. Whole-cell lysates were harvested and immunoprecipitated with the anti-FLAG antibody. The input and immunoprecipitates were analysed by WB with the indicated antibodies.

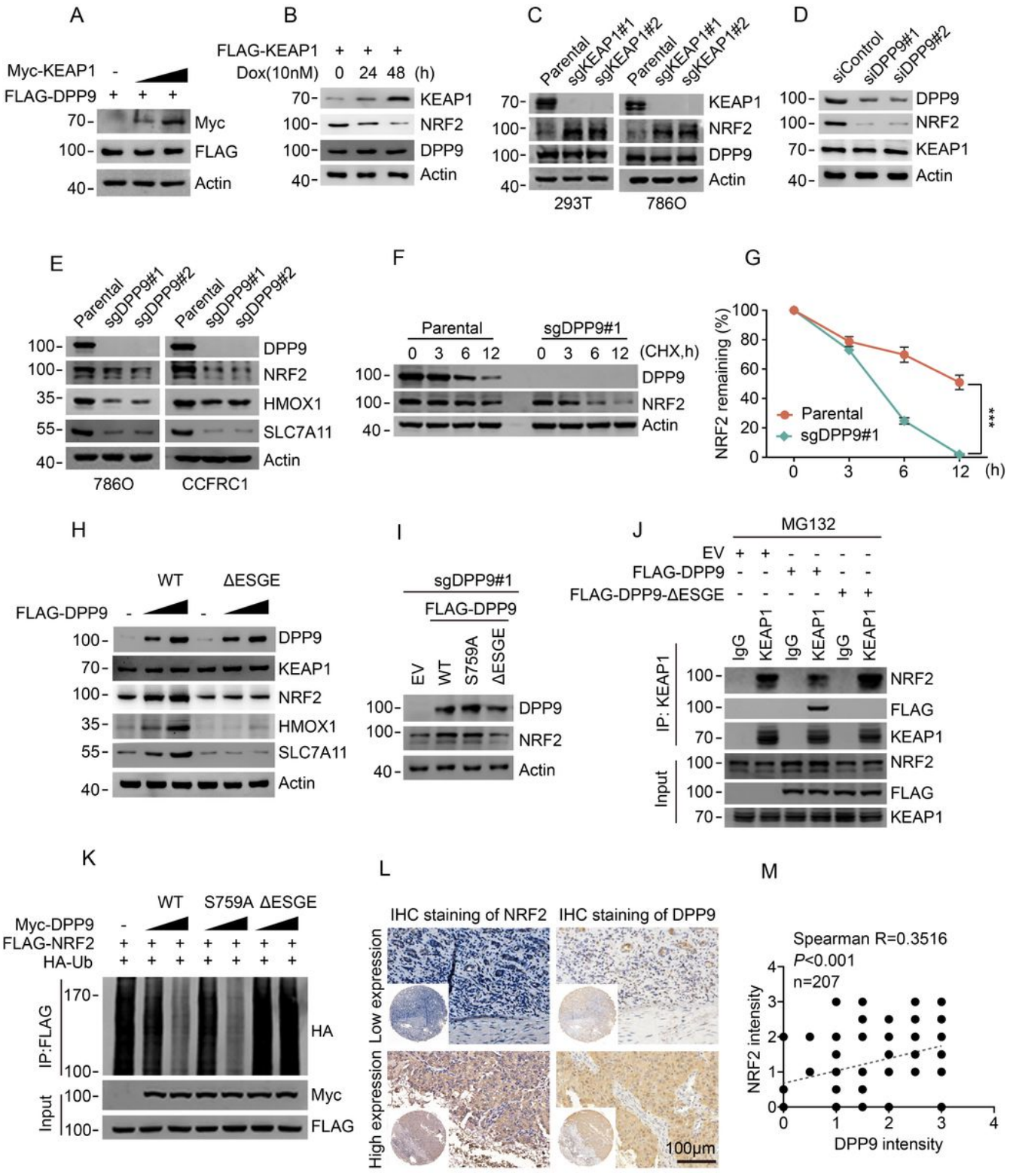

Figure 3

DPP9 promotes the stability of NRF2 and nuclear accumulation by competitively binding KEAP1.

(**A**) WB showed the effects of overexpressing KEAP1 on the protein level of ectopically co-expressed DPP9 in 786O cells.

(**B**) WB showed the effects of overexpressing KEAP1 on the protein levels of endogenous DPP9 and NRF2 in 786O cells. A doxycycline (Dox)-inducible Tet-On system was used for inducible KEAP1 expression in 786O cells.

(**C**) WB showed the effects of depleting KEAP1 by CRISPR/Cas9-mediated KO in 293T and 786O cells on the endogenous DPP9 and NRF2 protein levels.

(**D**) The effects of silencing DPP9 with siRNAs in 293T cells on the protein levels of endogenous KEAP1 and NRF2.

(**E**) WB analysis of the NRF2, HMOX1 and SLC7A11 protein levels in whole cell lysates from parental, DPP9 KO 786O and CCFRC1 cells.

(**F**, **G**) Parental and DPP9 KO 786O cells were treated with cycloheximide (CHX, 50 μg/ml) for the indicated times. NRF2 protein levels were analysed by WB (**F**). Quantitative data were taken from three independent experiments (**G**).

(**H**) WB showed the effect of the ESGE domain in DPP9 on the NRF2, HOMX1 and SLC7A11 protein levels in 786O cells.

(**I**) WB showed the effect of enzymatic activity and the ESGE domain of DPP9 on the NRF2 protein level (by transfecting DPP9-WT, the DPP-S759A mutant or the DPP-ΔESGE mutant into DPP9-KO 786O cells).

(**J**, **K**) DPP9 exerts its effects by competitive binding to KEAP1 (**J**) and protecting NRF2 from KEAP1-mediated degradation of ubiquitination (**K**).

(**L**, **M**) IHC analysis of the correlation between DPP9 and NRF2 protein levels in the FUSCC ccRCC cohort. Representative staining results of low and high expression of NRF2 and DPP9. Scale bars, 100 μm. (**L**). Summary of the quantification analysis (**M**).

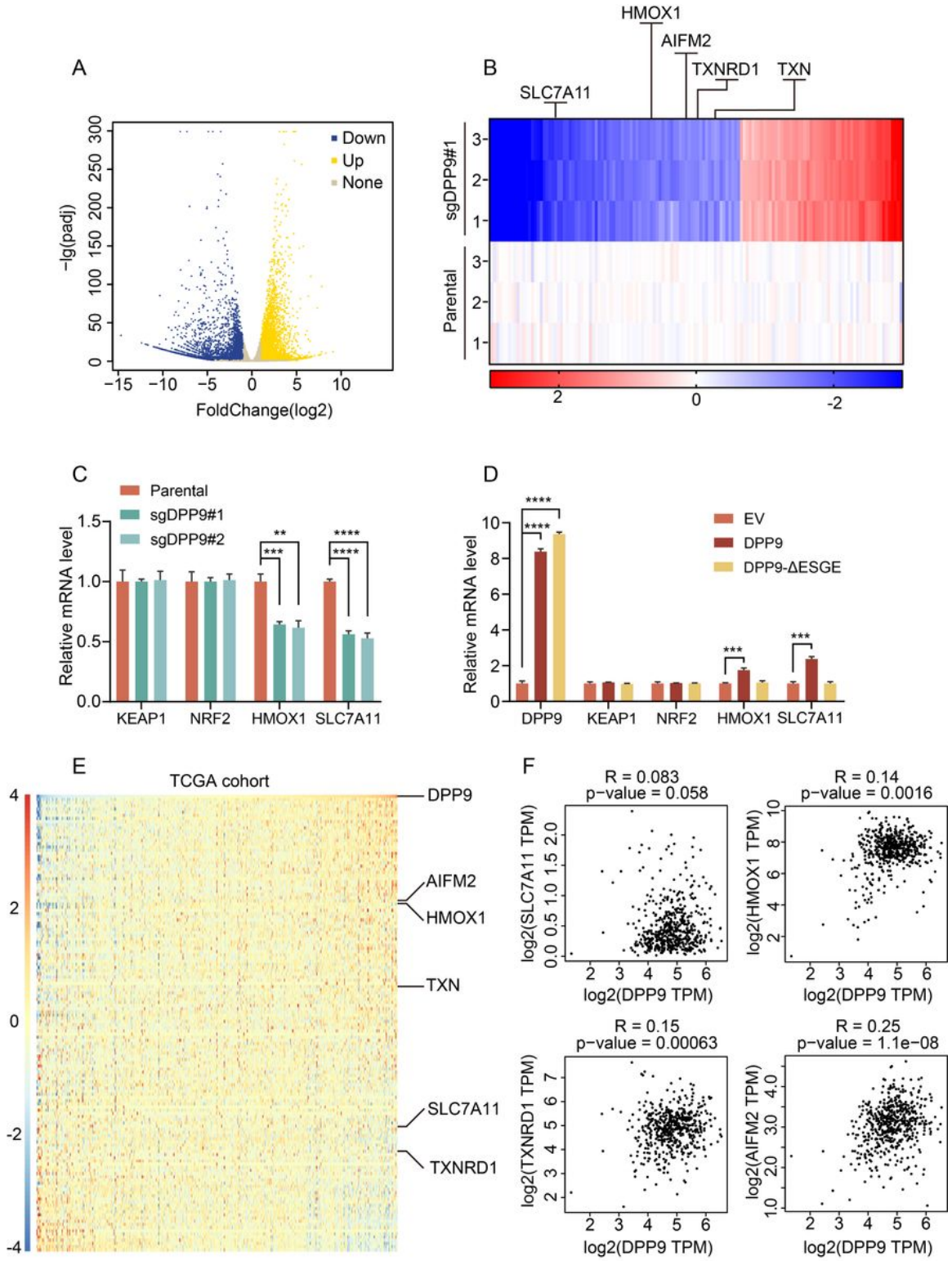

Figure 4

DPP9 enhances the transcriptional outputs of the NRF2 pathway.

(**A**) Volcano plot of the differentially expressed genes in parental and DPP9 KO 786O cells.

(**B**) Heatmap comparing the expression status of the 322 NRF2 downstream target genes between DPP9-KO 786O and parental cells.

(**C**) qRT-PCR showed HMOX1 and SLC7A11 mRNA changes in parental and DPP9 KO 786O cells.

(**D**) qRT-PCR showed HMOX1 and SLC7A11 mRNA changes in 786O cells overexpressing DPP9-WT or the DPP9-ΔESGE mutant.

(**E**) Heatmap illustrating the correlation between DPP9 expression and 322 NRF2 downstream target genes in the RNA-seq dataset from the TCGA ccRCC cohort.

(**F**) Representative status of DPP9 expression and several NRF2 downstream target genes.

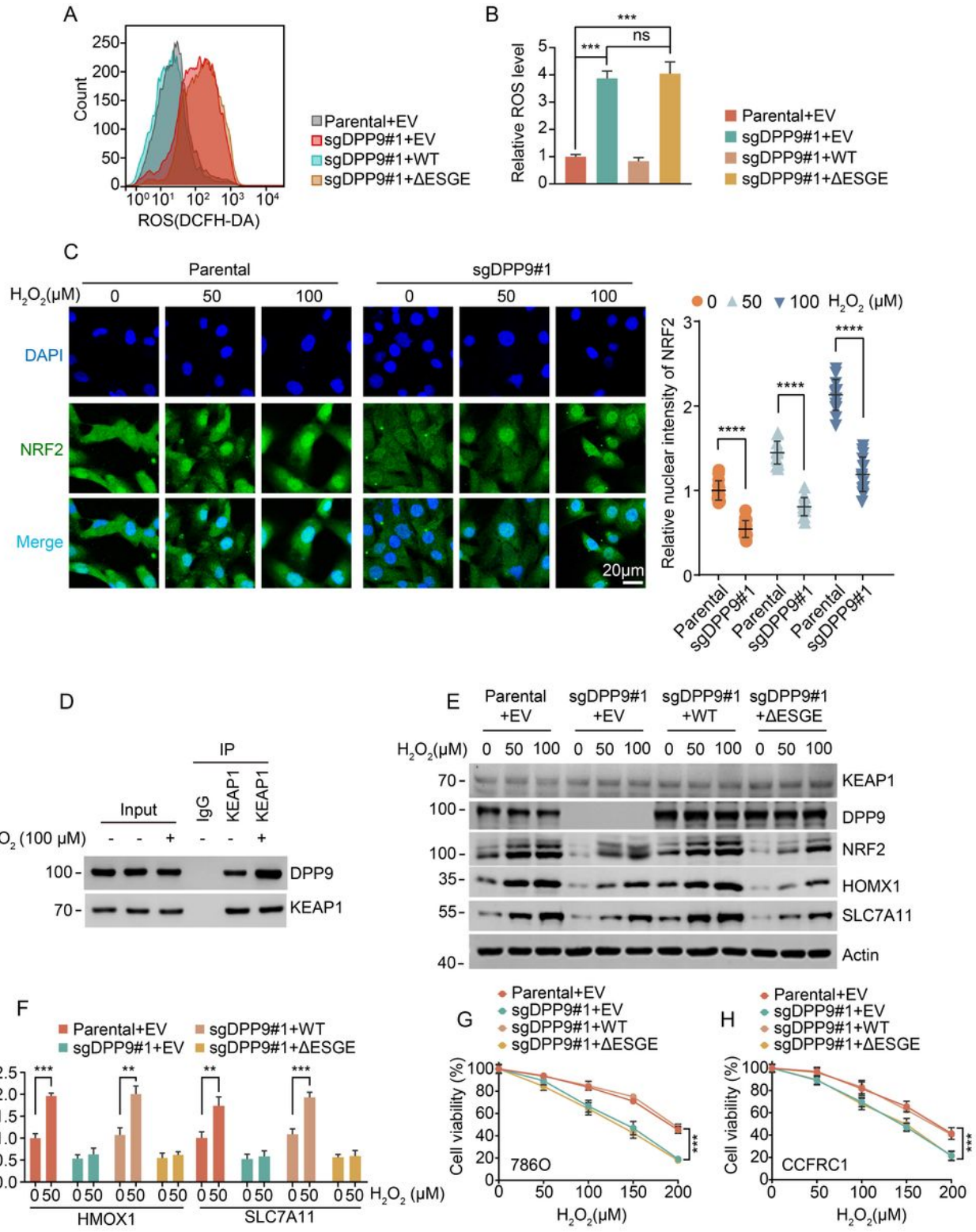

Figure 5

DPP9 regulates cellular ROS levels in a KEAP1-binding-dependent manner.

(**A**, **B**) Effects of DPP9-KO and the DPP9-ΔESGE mutant on ROS levels in 786O cells. The left panel is a representative image. The quantitative data are shown in (B).

(**C**) IF showed nuclear translocation of NRF2 in parental and DPP9 KO 786O cells after treatment with different concentrations of H_2O_2. The left panel shows the representative immunofluorescence images. Blue, DAPI; green, NRF2; scale bar, 20 μm. The nuclear NRF2 intensities of the cells shown in the left panel were quantified using ImageJ (right panel). About 15 cells from five or six random fields were analysed. Similar results were obtained from three independent experiments.

(**D**) The effect of H_2O_2 treatment (100 μM) on the interaction between KEAP1 and DPP9 in 786O cells. Whole-cell lysates were harvested and immunoprecipitated with the KEAP1 antibody. The input and immunoprecipitates were analysed by WB with the indicated antibodies.

(**E**, **F**) WB (**E**) and qRT-PCR (**F**) showed the expression levels of NRF2, HOMX1 and SLC7A11 in response to different H_2O_2 concentrations in parental and DPP9 KO cells, and the reintroduction of DPP9-WT or DPP9-ΔESGE mutant 786O cells.

(**G**, **H**) CCK-8 assays showed cell viability in parental and DPP9-KO cells, and reintroduction of DPP9-WT or the DPP9-ΔESGE mutant 786O (**G**) and CCRFC1 (**H**) cells after treatment with different H_2O_2 concentrations. All data are means ± standard deviations from three independent experiments.

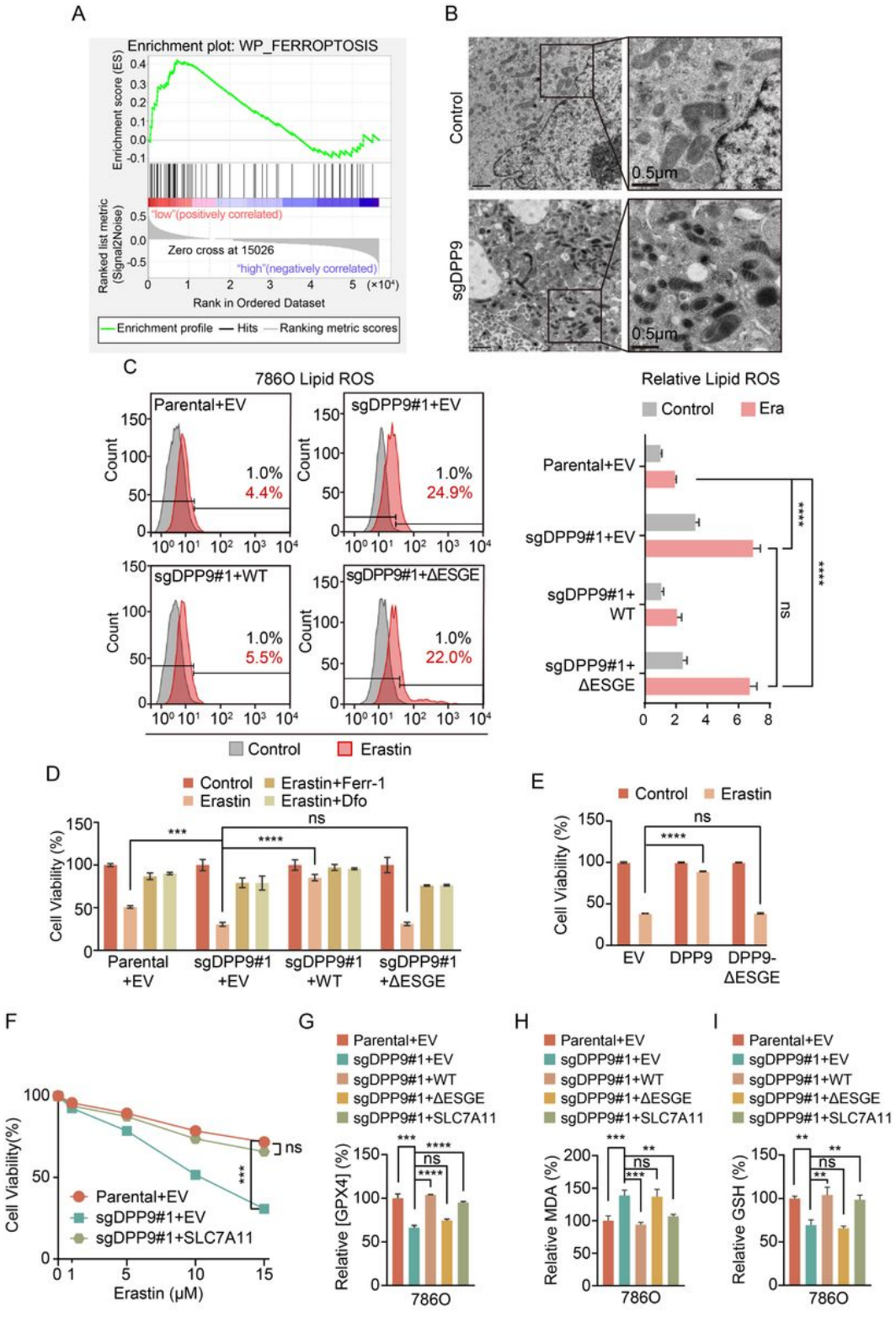

Figure 6

DPP9 overexpression contributes to suppress ferroptosis in a SLC7A11-dependent manner.

(A) GSEA of the ferroptosis gene signature in the parental and DPP9 KO 786O cells. The hallmark ferroptosis-related gene set was obtained from the Molecular Signatures Database (MsigDB).

(**B**) Electron microscopic analysis of morphological changes in the mitochondria of DPP9 KO 786O cells. Scale bars are 1 μm and 0.5 μm in the left and right photographs, respectively.

(**C**) Liperfluo staining was performed to monitor lipid ROS in parental, DPP9-KO and DPP9-WT or DPP9-ΔESGE mutant 786O cells. The left panel shows the representative fluorescence signals detected by flow cytometry. The relative lipid ROS levels of these cells are shown in the right panel. All data are means ± standard deviations from three independent experiments.

(**D**) CCK-8 assays showed erastin-induced cell death in cells treated with Ferr-1 (2 μM) and DFO (20 μM) for 24 h.

(**E**) CCK-8 assays showed erastin-induced cell death in 786O cells overexpressing DPP9-WT or ΔESGE mutant.

(**F**) CCK-8 assays showed the effect of SLC7A11 on erastin-induced cell death in DPP9 KO 786O cells.

(**G–I**) The effects of restoring DPP9-WT, ΔESGE mutant or SLC7A11 expression on the enzymatic activity of GPX4 (**G**), the levels of MDA (**H**) and cellular GSH (**I**).

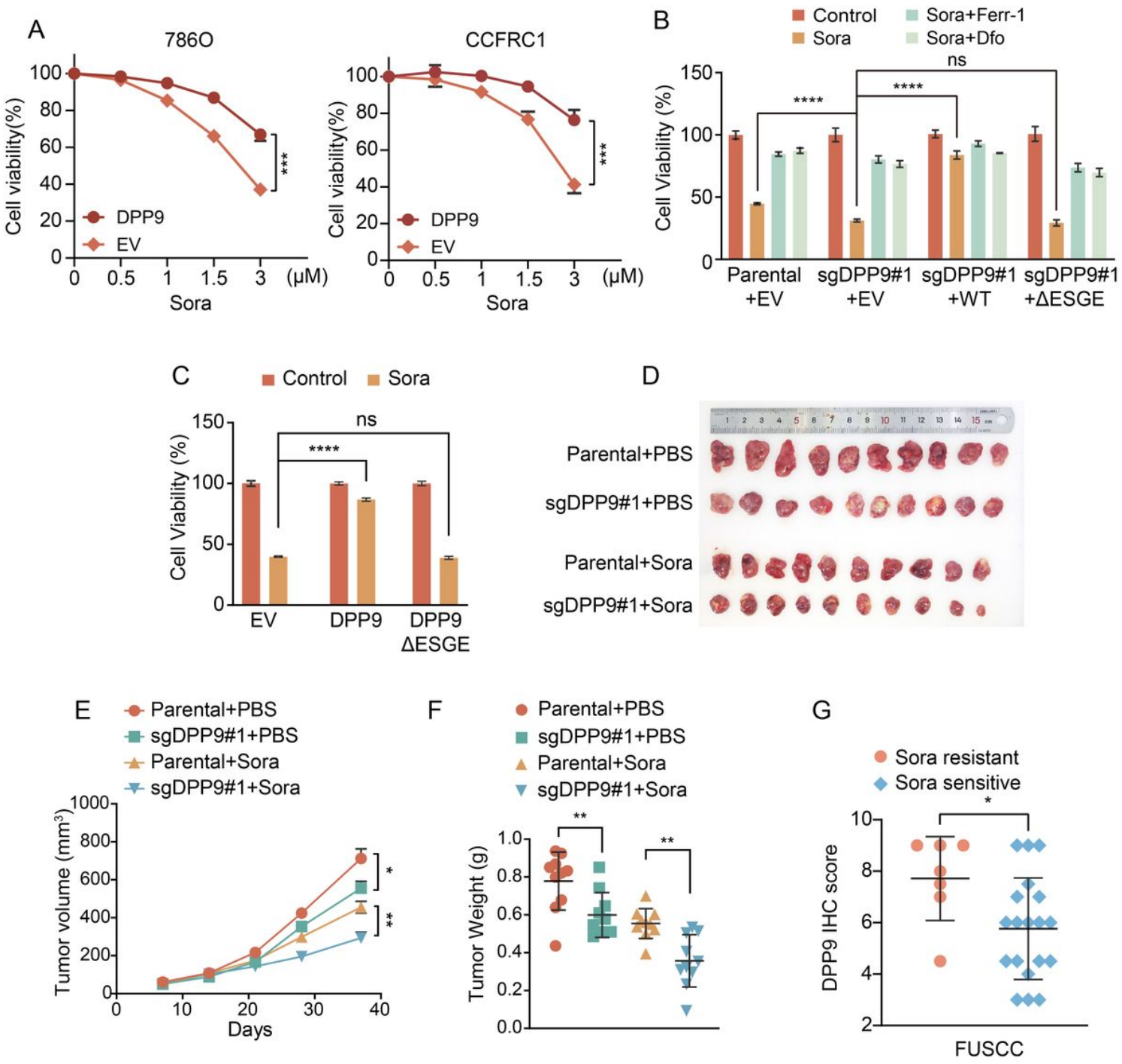

Figure 7

DPP9 overexpression contributes to sorafenib resistance in ccRCC.

(**A**) CCK-8 assays showed the response of sorafenib-induced cell death to DPP9 overexpressing 786O or CCF-FC1 cells. The cells were treated with the indicated concentrations of sorafenib for 24 h.

(**B**) CCK-8 assays showed the effects of Sora and Ferr-1 (or DFO) on cell death in parental, DPP9-KO, and reintroduction of the DPP9-WT or DPP9-ΔESGE mutant 786O cells. The concentrations of Sora, Ferr-1 and DFO were 3, 2 and 20 μM, respectively.

(**C**) CCK-8 assays showed the effects of DPP9-WT or the ΔESGE mutant overexpressed in 786O cells after the sorafenib treatment. The sorafenib concentration was 3 μM.

(**D**–**F**) A xenograft tumour model examining the role of DPP9 in sorafenib resistance. Photographs of the (**D**), volume (**E**) and weight (**F**) of the parental, DPP9-KO, sorafenib-treated parental and sorafenib-treated DPP9 KO 786O cell xenografts in nude mice are shown. Data are mean ± SD for each group of mice (N = 10).

(**G**) Comparison of DPP9 expression status between sorafenib-resistant and sorafenib-sensitive ccRCC patients from the FUSCC cohort.

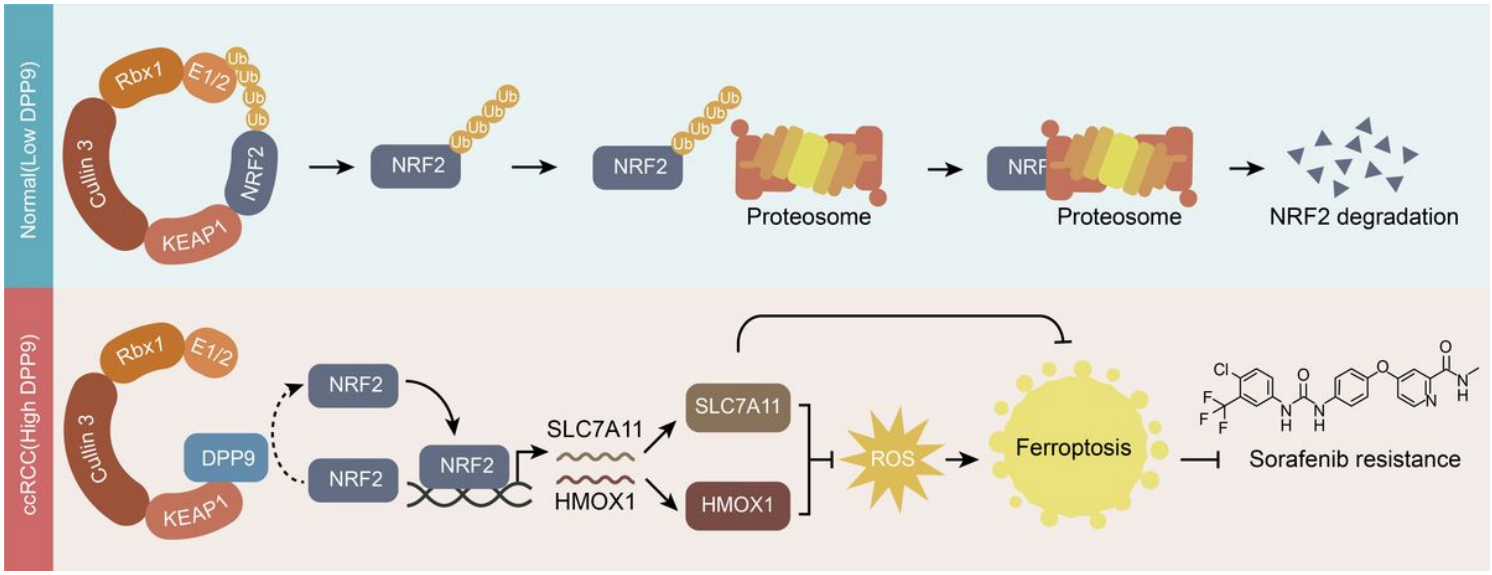

Figure 8

Model summarizing the findings of the present study.

Supplementary Files

This is a list of supplementary files associated with this preprint. Click to download.

- SupplementaryFigureseditted.docx
- SupplementaryTable1.xlsx
- SupplementaryTable2.xlsx
- SupplementaryTable3.xlsx
- SupplementaryTable4.xlsx